Kovove Mater. 57 2019 363–369
DOI: 10.4149/km_2019_5_363

Processing and characterization of porous SiC/NiTi alloys for biomedical applications

M. Şimşir, H. Akkan, K. E. Öksüz*

Department of Metallurgical & Materials Engineering, Sivas Cumhuriyet University, 58140, Sivas, Turkey

Received 16 May 2018, received in revised form 1 June 2019, accepted 3 June 2019

Abstract

NiTi shape memory alloys have attracted significant attention due to their unique shape memory effect, superelasticity, and excellent mechanical performance. In addition, the fact that NiTi alloys have high resistance to cavitation and corrosion makes them ideal candidate materials in advanced tribological and biomedical applications. The NiTi alloy composite reinforced by fine grain-sized SiC particles was successfully fabricated using powder metallurgy process. In this process, elemental Ni-Ti metal powder mixes reinforced with 0, 1, and 5 % SiC particulates were pressed uniaxial and sintered at 1100 °C in an argon atmosphere for 3 h. The effect of the SiC additions on the mechanical properties, porosity degree, and phase formation of the porous NiTi alloys was studied. After characterization, the bioactivity of the SiC/NiTi exposed samples was evaluated in simulated body fluid test. The microstructure characterization and phase identification of the apatite layer formed in SBF on their surface were also evaluated.

K e y w o r d s: NiTi alloys, silicon carbide, biocompatibility, porosity, wear mechanism

1. Introduction

The near equiatomic binary alloy, nickel-titanium (Nitinol) NiTi can reversibly change between two crystal structures. These two crystal structures are the low-temperature martensitic phase, which is monoclinic and has B19' symmetry, and the high-temperature austenitic phase that is cubic with B2' symmetry. The transformation between these two phases is responsible for the extraordinary mechanical properties which make the material so interesting. The reversible transformation upon loading and unloading is called pseudoelasticity. The ability to revert to an impressed high-temperature shape is called shape memory effect [1]. Materials with these extraordinary properties are often referred to as smart or intelligent materials. The interest in these materials for medical applications has been steadily growing during the last years [2]. NiTi shape memory alloys are reliable, functional materials widely used in various industrial applications as couplings, actuators, sensors, dental-medical devices, glasses frames, and for underwire bras due to their unique shape memory and superelasticity properties [3, 4]. The combination of these characteristics with good biocompatibility [5], coupled with the high mechanical response, has made NiTi alloys fabulous materials for dental and biomedical applications such as stents, orthodontic archwires, filters, and bone anchors [6, 7].

NiTi alloys have been fabricated using various powder metallurgy methods, such as self-propagating high temperature synthesis (SHS) [8, 9], conventional sintering (CS), [10, 11], hot isostatic pressing (HIP) [12], metal or powder injection molding (MIM) [13], spark plasma sintering (SPS) [14], and the space holder technique (SHT) [15–17]. The literature reviews have demonstrated that equiatomic NiTi alloy exhibits high mechanical and wear resistance. Some attempts were made previously to develop NiTi matrix composites [18, 19]. However, a very limited study with reinforcement powders was used for manufacturing NiTi alloys. In this study, the porous NiTi reinforced by fine grain-sized SiC particles, i.e., the SiC/NiTi composite, was fabricated by powder metallurgy process. The microstructure, phase formation, mechanical behavior (hardness and wear) and bioac-

*Corresponding author: e-mail address: kerimemreoksuz@gmail.com

tivity test of the SiC/NiTi composite were studied.

2. Experimental study

Nickel and Titanium powder (45 µm, 99.9 % purity) with an atomic ratio of 50.8 % Ni to 49.2 % Ti were mixed for 12 h. Afterward, fine grain-sized SiC particles (< 10 µm, 99.5 % purity) with weight fractions of 1 and 5 % respectively were added to the mixed Ni-Ti powder and blended for 12 h. Then, the sufficiently blended powders were cold compacted into short-bar green samples (6 mm × 10 mm, diameter × height) with compact stress of 500 MPa for 2 min. The compacted green samples were heated to 1100 ℃ and held for 3 h in an aluminum oxide tube furnace under the protective flowing argon gas (99.99 % purity). Sintered porous specimens were cooled in the cold zone of the furnace at a rate of approximately 5 ℃ min^{-1}, sufficient to prevent the formation of intermetallic other than NiTi due to possible oxidation problems that may occur during furnace cooling.

The porosity and bulk densities of the fabricated samples were measured by the Archimedes' principle. The pore feature and microstructure of the samples were characterized by field emission gun scanning electron microscopy (FE-SEM, Tescan Mira$_3$ XMU, Czech Republic) equipped with energy-dispersive X-ray spectroscopy (EDS) following phase constituent analysis using Philips (Rigaku D/MAX/2200/PC) XRD. The microhardness of the composite and its alloy were measured by Vickers hardness (Schimadzu® MHV tester) method, and the mean of at least eight readings was taken. A pin-on-disc type of apparatus was employed to evaluate the wear characteristics of the samples by the ASTM G99 test standard. Wear tests were carried out at room temperature without lubrication. In wear tests, normal loads on the pin were 20, 40, and 60 N at a constant sliding speed of 1 m s^{-1} and a constant sliding distance of 60 m for each sample. The test samples were sliding against SiC papers. Each test was performed with a fresh SiC paper 180 grits, which is corresponding to ∼ 70 µm. The samples were wholly cleaned by acetone before and after each test and weighted using a digital balance with an accuracy of ± 0.1 mg. The average values of three repeated experiments were referred. To evaluate and compare the bioactivity characteristics in terms of apatite-forming capability, NiTi samples were immersed in 1.5 × simulated body fluid (SBF). Samples were vertically soaked in 120 ml of SBF in closed screw-capped polypropylene bottles for 7, 14, and 21 days. The 1.5 × SBF was prepared by dissolving reagent-grade chemicals of NaCl, $NaHCO_3$, KCl, Na_2HPO_4, $MgCl_2 \cdot 6H_2O$, $CaCl_2 \cdot 2H_2O$, and Na_2SO_4 in deionized water buffered at pH 7.40 with $((CH_2OH)_3CNH_2)$ and 1.0 mol l^{-1} HCl at 36.5 ± 0.5 ℃ [20]. The SBF was refreshed every second day to maintain constant ion concentrations. After soaking for 7, 14, and 21 days, samples were removed from SBF and gently rinsed with distilled water. Before characterization by SEM and EDS, samples were dried in air at room temperature.

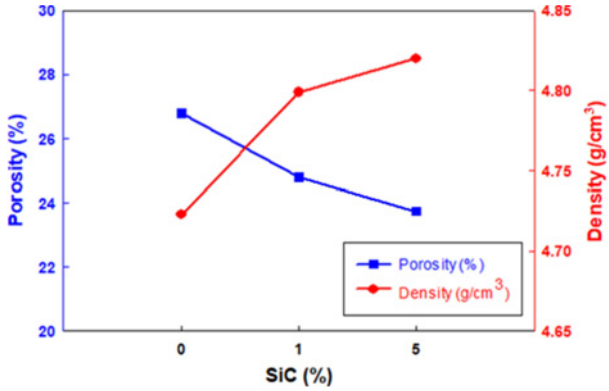

Fig. 1. The porosity and bulk density of SiC/NiTi composites.

3. Results and discussion

3.1. Density and porosity measurements

The vacuum method (European Norm EN 14411) was used in the laboratory to determine porosity and bulk density with greater precision. The porosity and bulk density are compared in Fig. 1.

It follows from above that both porosity and density of 5%SiC/NiTi are different from those of 0%SiC/NiTi's. The highest bulk density of NiTi composites (with 5 % SiC) was measured to be 4.825 g cm^{-3} and the corresponding porosity was 23.75 %. When we compared the relative density of 5%SiC/NiTi sample, which has the highest density, with that of commercial NiTi alloy ($\rho_s = 6.45$ g cm^{-3}), we found that the relative density of 5%SiC/NiTi sample is 25.2 % less [16]. In addition, it could be observed that the relative density of 0%SiC/NiTi sample is 73.2 %, 74.4 % for 1%SiC/NiTi, and 74.8 % for 5%SiC/NiTi.

3.2. Microhardness and wear performance of SiC/NiTi composites

The Vickers hardness value (VHN) was measured at a load of 1.96 N for the SiC/NiTi composites. The hardness values tend to increase due to the increasing amount of SiC in NiTi matrix to form more ceramic phases around grain boundaries [10].

By increasing SiC content, the densification was almost completed. The hardness for 0%SiC/NiTi,

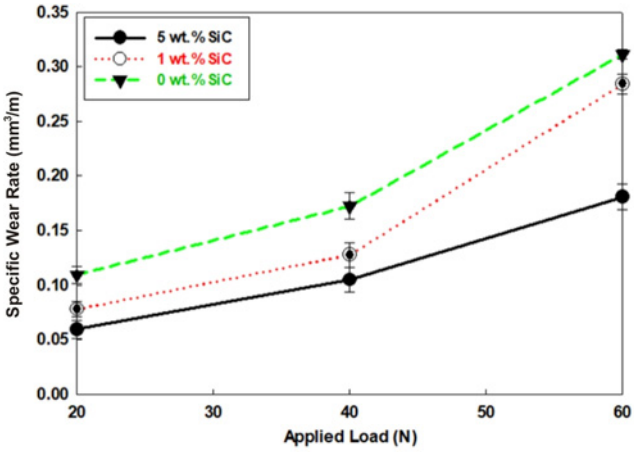

Fig. 2. The influence of the applied load on the wear rate of SiC particle-reinforced NiTi alloys.

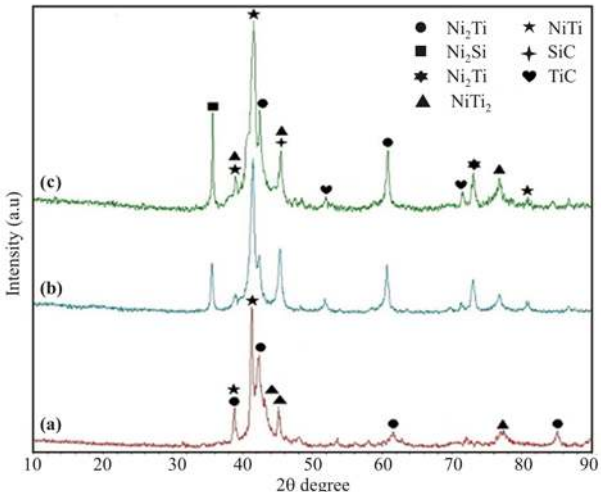

Fig. 3. XRD spectrum of (a) 0%SiC/NiTi, (b) 1%SiC/NiTi, and (c) 5%SiC/NiTi.

1%SiC/NiTi, and 5%SiC/NiTi composite are about 459.42 VHN, 777.6 VHN, and 827 VHN, respectively. This situation can be attributed to the increasing silicon carbide content and dissolution of more Ni-Ti phases into grains and grain boundaries. These results indicated that the hardness of the composites increased with increasing the content of particles up to 5 wt.%. The specific wear rate of SiC/NiTi composites is illustrated graphically in Fig. 2 as a function of different loads. The volume loss was calculated in terms of a specific wear rate. The specific wear rate is the volumetric loss per unit distance. The volume loss was calculated as:

$$\Delta V = \frac{\Delta m}{\rho} \times 1000, \tag{1}$$

where ΔV is the volume loss in (mm^3), Δm is the mass loss in (g), and ρ is the density of the composite in ($g\,cm^{-3}$). Specific wear rate $K = \frac{\Delta V}{d}$, where d is sliding distance, and for each specimen, it is kept constant = 60 m. It was found that the specific wear rate of the composites increases with applied load for all testing materials. In the SiC/NiTi composites, there was a stable behavior between 20 and 60 N loads. Significant increase in wear rate of the composite was observed. One reason is that ultra-fine sized SiC particles prevent the movement of dislocations in the NiTi matrix through a dispersion-strengthening mechanism [10]. Also, 5 wt.% SiC particle-reinforced NiTi demonstrated lower wear than that of unreinforced NiTi composites for all applied loads.

3.3. Microstructure and phase formation of SiC/NiTi alloy and its composites

Figure 3 shows XRD patterns of SiC/NiTi composites with different fractions of SiC. At room temperature, 0%SiC/NiTi mainly consists of NiTi phase and some second phases, such as Ni_4Ti_3, $NiTi_2$, and Ni_3Ti. Four crystalline phases, namely Ni_2Si, SiC, TiC, and Ni_2Ti with varying peak intensities, could be detected in patterns by increasing SiC content. In all cases, the diffractograms have predominantly registered the phase of NiTi, matched for every sample. For NiTi alloy (0%SiC), according to the Ni-Ti binary phase diagram, NiTi, $NiTi_2$, and Ni_3Ti can form easily during sintering at temperatures up to 1000 °C and become stable compounds. For 1 wt.%-SiC and 5 wt.%-SiC particle-reinforced NiTi, Gibbs free energies of Ni_2Si (–142.7 kJ mol^{-1}) and TiC (–184.1 kJ mol^{-1}) are lower than that of SiC (–71.4 kJ mol^{-1}) at 700 °C and above, indicating the high thermodynamic driving force of formation of Ni_2Si and TiC which in turn decrease the Ni content of the NiTi matrix during the sintering process [21, 22]. Decreasing the Ni content of the NiTi matrix restrains the formation of Ni_3Ti, so Ni_2Ti forms during the sintering process.

The internal morphology of the NiTi alloys was examined by FEG-SEM (SEI) equipped with an EDS. Figures 4a–d show the internal morphology image of the NiTi alloys with different ratios of SiC. Figure 4a shows a general view of the 5%SiC/NiTi alloy structure as a secondary electron image. In Fig. 4a many irregular and closed pores can be seen in the composite matrix. Figures 4b–d show backscattered electron images of 0%SiC/NiTi, 1%SiC/NiTi and 5%SiC/NiTi, respectively. Three phases (marked arrow) may be recognized by their respective shading contrast. The dark phase was identified to be NiTi and $NiTi_2$, the gray phase Ni_2Ti, and the bright phase Ni_3Ti.

The observation of the co-existence of NiTi, $NiTi_2$, and Ni_3Ti in the equiatomic sample is consistent with previous studies [23–25]. However, this is not expected, according to the Ti-Ni equilibrium phase

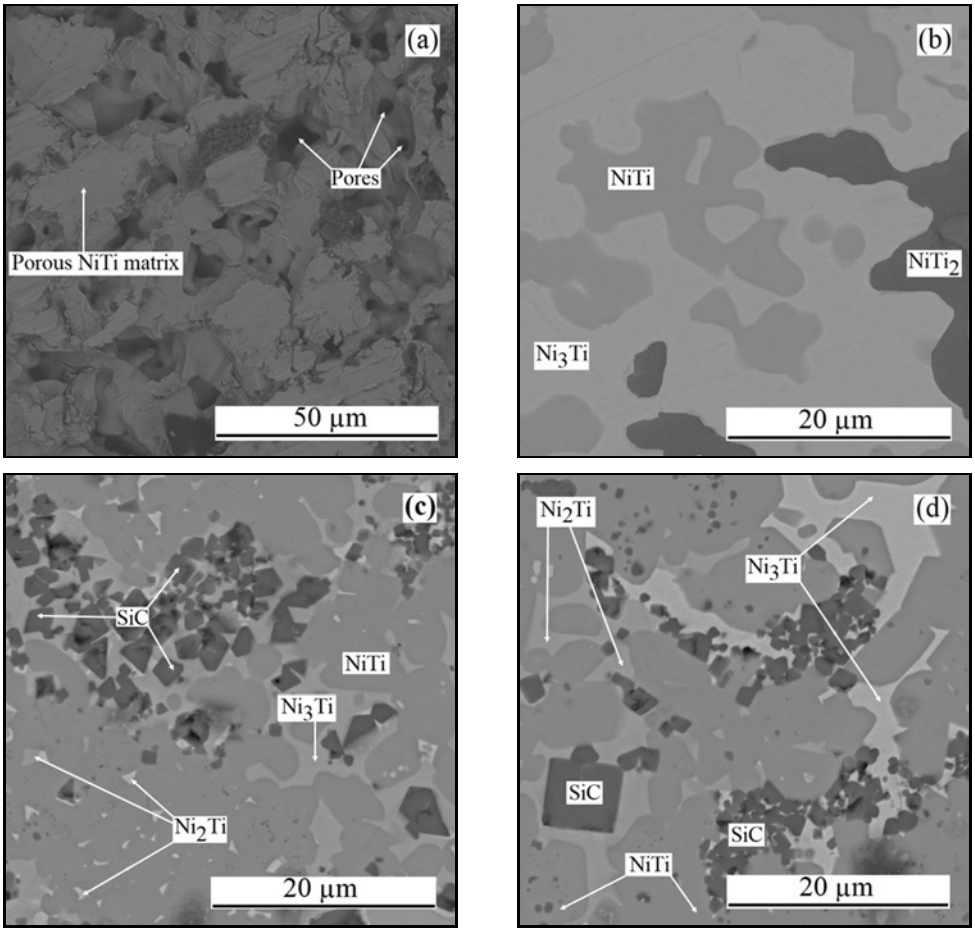

Fig. 4. Internal morphology images of (general view) of (a) 5%SiC/NiTi, (b) 0%SiC/NiTi, (c) 1%SiC/NiTi, and (d) 5%SiC/NiTi.

diagram. To explain this, several studies have been proposed in the literature. The researchers considered that the formation and the co-existence of the three phases are controlled by solid-state diffusion reactions between Ni and Ti. Regardless of the uniformity or the total composition of the mixing, locally the condition is always diffusion between pure Ti and pure Ni at the beginning of the sintering reaction process. In this regard, NiTi is not formed directly by interdiffusion between Ni and Ti. NiTi can only be formed by the interaction between Ni_3Ti and $NiTi_2$. In line with this discussion, Ni_3Ti (major phase) and $NiTi_2$, NiTi phases were formed in the matrix of 0%SiC/NiTi. A large number of, Ni_2Ti, $NiTi_2$ and dark-gray SiC--based particles (indicated by the arrow in Figs. 4c,d) exist in the matrix of 1%SiC/NiTi and 5%SiC/NiTi. The dark-gray SiC-based particles have complicated compositions related to $NiTi_2$, Ni_2Si, TiC, and residual SiC particles, as confirmed by EDS and XRD results.

3.4. Apatite-forming ability test

The surface appearances of the samples immersed in SBF for 7, 14, and 21 days are shown in SEM micrographs in Fig. 5. After 7 days soaking in SBF, there were many calcium phosphate particles formed and an integrated calcium phosphate layer formed within 14 and 21 days soaking. Prolonged immersion in SBF encouraged apatite growth and full coverage of the oxidized surfaces while inducing crack formation within the smooth apatite layer. Figure 6 shows EDS patterns of calcium and phosphate formed on the surface of 0%SiC/NiTi and 5%SiC/NiTi samples for a different time. As pointed out in Fig. 6, few calcium phosphate particles deposited on SiC/NiTi. Calcium and phosphate peaks became more prominent after immersing for 14 and 21 days compared to 7 days of immersion in SBF for all tested samples.

However, complete coverage of the 5%SiC/NiTi surface with apatite layer was not observed even after a duration time of 7, 14, and 21 days. The surfaces of the SiC/NiTi samples (especially 5%SiC/NiTi) were covered with micron-sized, spherical precipitates, which were not rich in calcium and phosphorus as evidenced by EDS analysis conducted during SEM surveys. After a duration time of 21 days, XRD analysis showed that the intensity of the peak of TiO_2 (rutile)

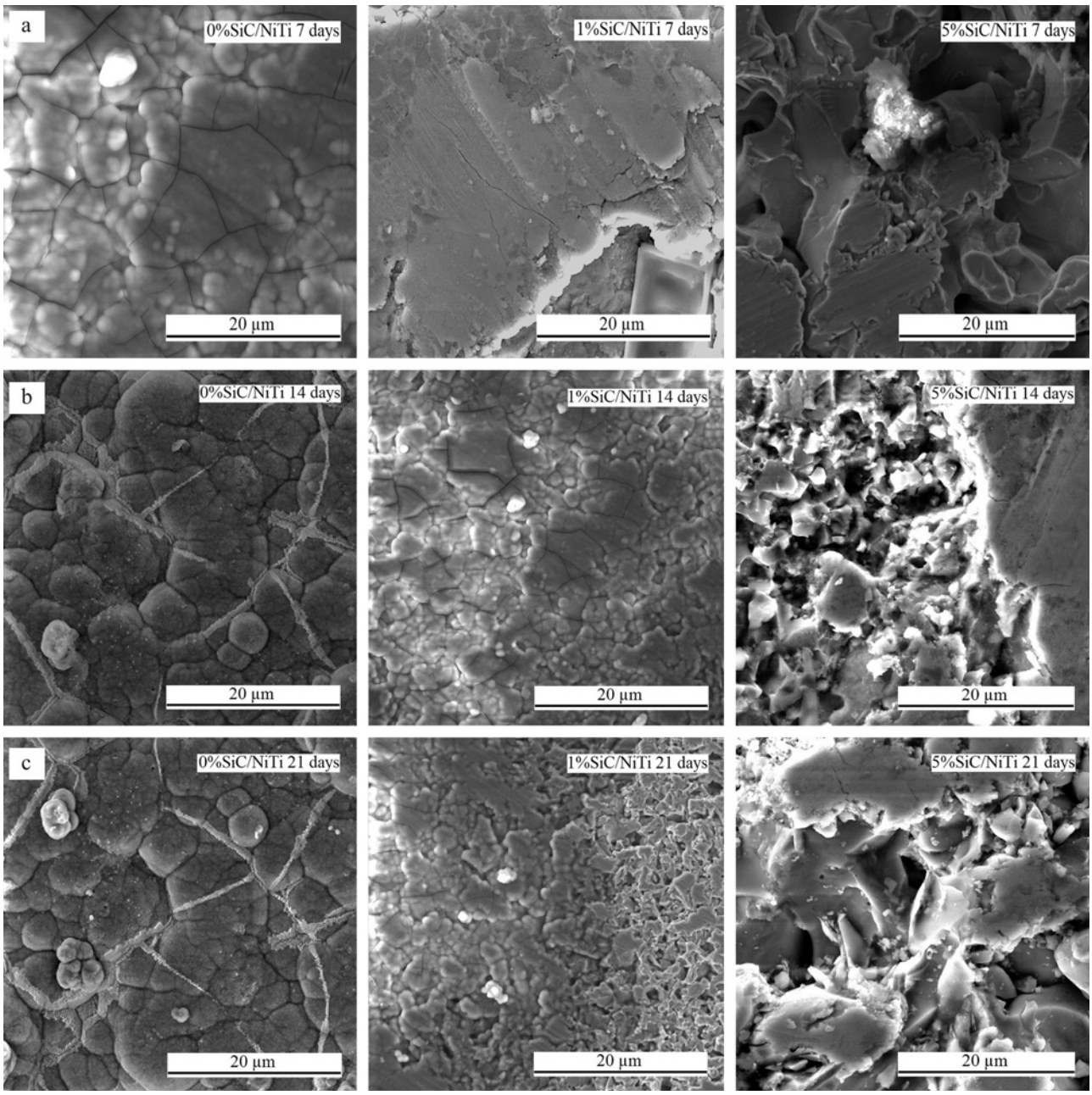

Fig. 5. Surface morphologies of SiC/NiTi samples immersed in SBF for (a) 7, (b) 14, and (c) 21 days.

phase slightly decreased, while broad HA peaks appeared in between $2\theta \cong 30°$–$36°$ on the XRD spectrum (not showed). Accelerated biomimetic apatite precipitation on NiTi samples can be associated with the hydrolysis of the outermost biocompatible compound layer leading to supersaturation of SBF with Ca^{2+}, OH^-, TiO $(OH)_2$ and HPO_4^{2-} ions at the vicinity of the exposed surface [26].

The reactivity of these ionic components stimulates rapid nucleation and growth of apatite on the oxide layer [26]. Moreover, it has been reported that 0%SiC/NiTi imposed surfaces promote more suitable sites for biomimetic apatite precipitation owing to their porous and rough nature [27]. As confirmed by the existence of the Ca-P-O related peaks as seen in EDS at 3.69, 2.03, and 0.52 keV, respectively, the HA peaks can be derived from EDS peaks. The biomimetic growth mechanism in SBF may be associated with fine crystallite apatite precipitation as seen from SEM figures. Longer durations in SBF induced thick, but cracked apatite layer formation. Previously, cracking of the apatite layer was attributed to the capillary stresses arising from the evaporation of entrapped water in apatite during drying of the samples after removing from the SBF [20]. Finally, the results of the SBF tests can be taken as the primary indicator of su-

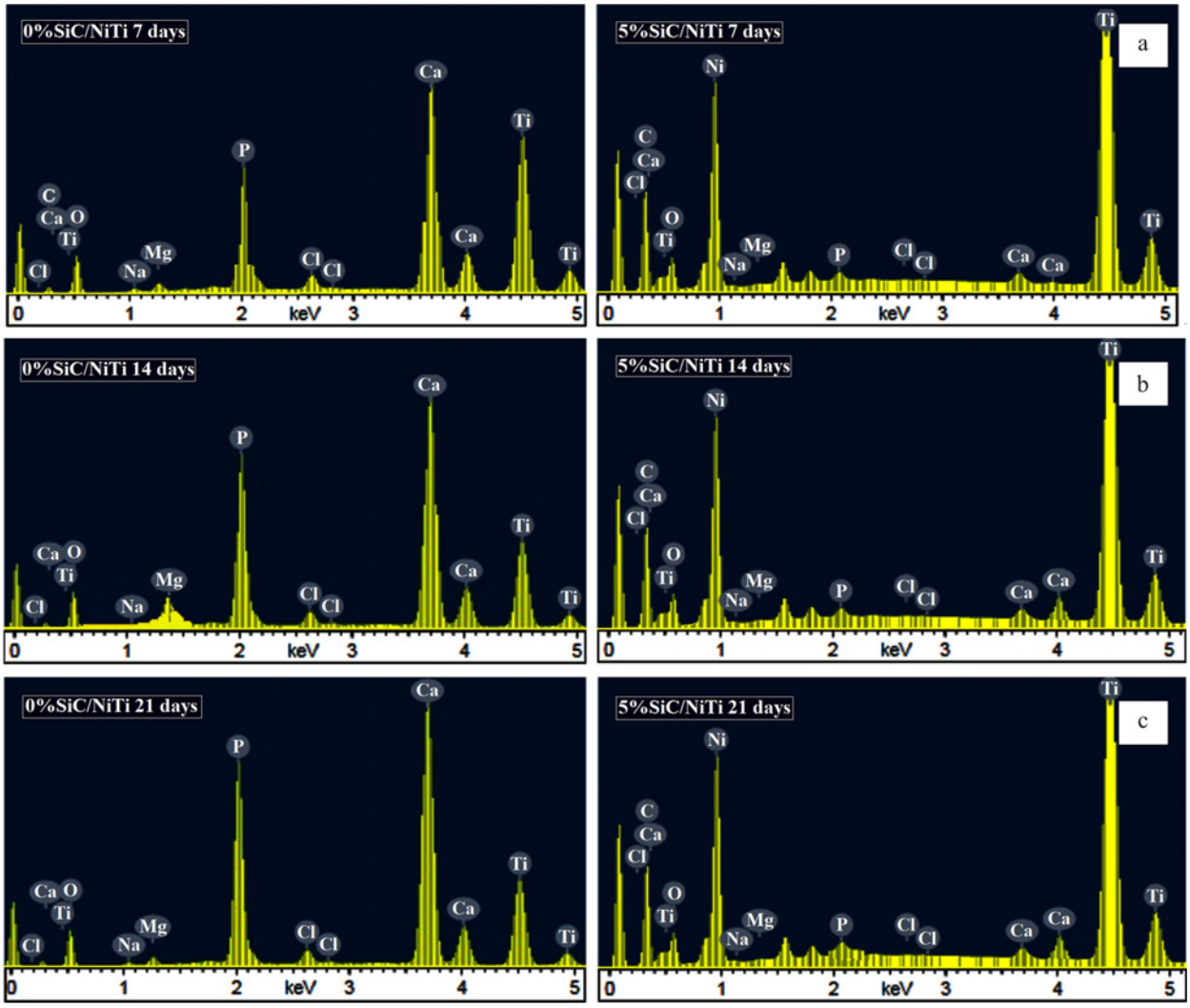

Fig. 6. EDS spectra of the 0%SiC/NiTi and 5%SiC/NiTi samples immersed in SBF for (a) 7, (b) 14, and (c) 21 days.

perior biochemical binding between bone and the surfaces of the 0%SiC/NiTi and the 1%SiC/NiTi samples in comparison to that of the 5%SiC/NiTi.

4. Conclusions

The fine grain-sized SiC particle reinforced NiTi alloy composite with low density and high hardness was successfully fabricated by a powder metallurgy process. The distribution of SiC particles leads to a change of phase constituents of the NiTi matrix. As the amount of SiC particles increase, the composite's densification declines. Also, as the SiC particles increase up to 5 % in the NiTi samples, porosity increases. Increasing the amount of SiC promotes high hardness and wear resistance in the NiTi alloy. According to SEM micrographs, the SiC/NiTi alloys show a uniform microstructure in which silicon carbide particles are distributed evenly in the NiTi matrix. After the SBF test, SEM and EDS analysis results confirm that the layer formed on the surface of the oxide layer is apatite. These features show that the oxide layer on the SiC/NiTi alloy can induce the bone-like apatite nucleation and growth on their surfaces from SBF. Bone-like apatite is found to be essential to establish the bone-bonding interface between bioactive materials and living tissues. The obtained material may be suitable for dental implants and prostheses after *in-vivo* tests.

References

[1] Buehler, W. J., Wang, F. E.: Ocean Eng., *1*, 1968, p. 105. doi:/10.1016/0029-8018(68)90019-X

[2] Huang, H. H., Chiu, Y. H., Lee, T. H., Wiu, S. C., Yang, H. W., Su, K. H., Hsu, C. C.: Biomaterials, *24*, 2003, p. 3585. doi:/10.1016/S0142-9612(03)00188-1

[3] Funakubo, H.: Shape Memory Alloys. Amsterdam, Gordon and Breach Science Publishers S. A. 1987.

[4] Otsuka, K., Wayman, C. M.: Shape Memory Materials. Cambridge, Cambridge University Press 1998.
[5] Shabalovskaya, S.: Bio-Med Mater. Eng., *6*, 1996, p. 267. doi:10.3233/BME-1996-6405
[6] Itin, V., Gyunter, V., Shabalovskaya, S., Sachdeva, R.: Mater. Charact., *32*, 1994, p. 179. doi:10.1016/1044-5803(94)90087-6
[7] Pelton, A. R., Stoeckel, D., Duerig, T. W.: Mater. Sci. Forum, *328*, 2000, p. 63. doi:10.4028/www.scientific.net/MSF.327-328.63
[8] Yuan, B., Zhang, X. P., Chung, C. Y., Zeng, M. Q., Zhu, M.: Metall. Mater. Trans. A, *37*, 2006, p. 755. doi:10.1007/s11661-006-0047-5
[9] Tosun, G., Özler, L., Kaya, M., Orhan, N.: J. Alloys Compd., *487*, 2009, p. 605. doi:10.1016/j.jallcom.2009.08.023
[10] Şahin, Y., Öksüz, K. E.: JOM, *66*, 2014, p. 61. doi:10.1007/s11837-013-0823-9
[11] Zhu, S. L., Yang, X. J., Fu, D. H., Zhang, L. Y., Li, C. Y., Cui, Z. D.: Mater. Sci. Eng. A, *408*, 2005, p. 264. doi:10.1016/j.msea.2005.08.012
[12] Greiner, C., Oppenheimer, S. M., Dunand, D. C.: Acta Biomater., *1*, 2005, p. 705. doi:10.1016/j.actbio.2005.07.005
[13] Guoxin, H., Lixiang, Z., Yunliang, F., Yanhong, L.: J. Mater. Process. Techn., *206*, 2008, p. 395. doi:10.1016/j.jmatprotec.2007.12.044
[14] Zhao, Y., Taya, M., Kang, Y. S., Kawasaki, A.: Acta Mater., *53*, 2005, p. 337. doi:10.1016/j.actamat.2004.09.029
[15] Bansiddhi, A., Dunand, D. C.: Intermetallics, *15*, 2007, p. 1612. doi:10.1016/j.intermet.2007.06.013
[16] Zhang, Y. P., Li, D. S., Zhang, X. P.: Scripta Mater., *57*, 2007, p. 1020. doi:10.1016/j.scriptamat.2007.07.043
[17] Bansiddhi, A., Dunand, D. C.: Acta Biomater., *4*, 2008, p. 1996. doi:10.1016/j.actbio.2008.06.005
[18] Ye, H. Z., Li, D. Y., Eadie, R. L.: Mater. Sci. Eng. A, *329–331*, 2002, p. 750. doi:10.1016/S0921-5093(01)01655-0
[19] Li, D. Y., Luo, Y.: J. Mater. Sci. Lett., *20*, 2002, p. 2249. doi:10.1023/A:1017909723229
[20] Jalota, S., Bhaduri, S. B., Taş, A. C.: J. Mater. Sci-Mater. Med., *17*, 2006, p. 697. doi:10.1007/s10856-006-9680-1
[21] Jackson, M. R., Mehan, R. L., Davis, A. M., Hall, E. L.: Metall. Trans. A, *14*, 1983, p. 355. doi:10.1007/BF02644213
[22] Touanen, M., Teyssandier, F. J., Ducarroir, M.: Mater. Sci. Lett, *8*, 1989, p. 98. doi:10.1007/BF00720264
[23] Burkes, D. E., Moore, J. J.: J. Alloys Compd., *430*, 2007, p. 274. doi: 10.1016/j.jallcom.2006.05.008
[24] Shuilin, W., Chung, C. Y., Xiangmei, L., Paul, K. C., Ho, J. P. Y., Chu, C. L., Chan, Y. L., Yeung, K. W. K., Lu, W. W., Cheung, K. M. C., Luk, K. D. K.: Acta Mater., *55*, 2007, p. 3437. doi:10.1016/j.actamat.2007.01.045
[25] Bidaux, J. E., Neudenberger, M., Bertherville, B.: Mater. Sci. Eng. A, *384*, 2004, p. 143. doi:10.1016/j.msea.2004.06.025
[26] Song, W. H., Jun, Y. K., Han, Y., Hong, S. H.: Biomaterials, *25*, 2004, p. 3341. doi:10.1016/j.biomaterials.2003.09.103
[27] Wei, D., Zhou, Y., Yang, C.: Colloids Surf B: Biointerfaces, *74*, 2009, p. 23. doi:10.1016/j.colsurfb.2009.07.025